Materials Today Communications 32 (2022) 103906

Contents lists available at ScienceDirect

Materials Today Communications

journal homepage: www.elsevier.com/locate/mtcomm

Multifunctional hydrogels of polyvinyl alcohol/polydopamine functionalized with carbon nanomaterials as flexible sensors

Dinesh K. Patel [a], Keya Ganguly [a], Sayan Deb Dutta [a], Tejal V. Patil [b], Ki-Taek Lim [a,b,*]

[a] Department of Biosystems Engineering, Institute of Forest Science, Kangwon National University, Chuncheon 24341, Republic of Korea
[b] Interdisciplinary Program in Smart Agriculture, Kangwon National University, Chuncheon 24341, Republic of Korea

ARTICLE INFO

Keywords:
Carbon dots
Recovery strength
Adhesiveness
Conductivity
Strain sensing

ABSTRACT

The demand of multifunctional hydrogels has been significantly increased to develop wearable strain-sensing devices. However, integrating all desired properties into one component is still challenging. To address this, we developed polyvinyl alcohol (PVA)/polydopamine functionalized carbon dots (PDA@CDs) hydrogels for strain sensing application. The CDs were obtained from cucumber peels through a one-pot heat treatment process and characterized by different spectroscopic techniques. The PDA@CDs were synthesized *via* a pH-induced polymerization process. The addition of PDA@CDs improved the adhesiveness and conductivity of the PVA matrix. An improved mechanical, rheological, and recovery strength was observed in PDA@CDs incorporated hydrogels than the pure PVA hydrogel, demonstrating enhanced interactions among PVA and PDA@CDs. The PDA@CDs added hydrogels demonstrated superior near-infrared (NIR) responsive property, and a rapid enhancement in the temperature (31.3 °C → 123 °C) was observed in the developed hydrogels within 1 min of laser light (808 nm) irradiation at 1.5 W/cm^2. The developed hydrogels did not exhibit any toxic effects on human dermal fibroblasts (HDFs), suggesting their cytocompatibility. Furthermore, the antibacterial activity of the developed hydrogels was monitored with *Escherichia coli.* No bacteria colony was found on the surface of developed hydrogels, demonstrating their antibacterial potential. The sensing ability of the developed hydrogels was monitored at different parts of the human body (finger, wrist, and knee joint). These findings indicate that PDA functionalized CDs have effectively improved PVA properties and can be explored for wearable strain sensors.

1. Introduction

Various nature-inspired biomimetic multifunctional hydrogels have been developed for different applications [1]. The skin is the largest and outermost layer of the human body and acts as a barrier to microbial infections. The skin has autonomous self-healing potential and can sense different stimuli, including temperature, strain, vibration, and pressure [2]. Inspired by the natural skin properties, various bionic skin multifunctional materials have been developed to monitor human motion, body temperature, blood pressure, and analyte detection in body fluids [3–6]. Fabricating smart materials with adequate mechanical strength, rapid self-healing, and improved conductivity is a crucial challenge for flexible wearable electronic devices. Stretchable electronic devices have been widely utilized in sensing, soft robotics, energy harvesting, and bionic skin. Hydrogels are physically or chemically cross-linked three--dimensional polymeric structures with solid-like mechanical strength and liquid-like diffusion properties [7–10]. Conductive hydrogels with self-healing potential have received significant attention for the development of bionic skin owing to their improved recovery efficiency after deformation and tunable functions. Additionally, these materials should be biocompatible to use in bionic skin patches. Various elastomers such as polydimethylsiloxane (PDMS) or polyvinyl alcohol (PVA)-based hydrogels have been extensively utilized as stretchable substrates [7]. PVA-based hydrogels are widely explored in biomedical applications because of their easy synthesis, water-solubility, self-healing, biodegradability, and biocompatibility [11–13]. However, the broad applicability of PVA hydrogels is restricted owing to their weak mechanical strength and poor adhesiveness to tissue. These drawbacks can be overcome by blending other polymers or suitable nanomaterials in the PVA matrix [14,15].

Mussel-based polydopamine (PDA) materials have received considerable attention for sensing applications owing to their self-adhesiveness

* Corresponding author at: Department of Biosystems Engineering, Institute of Forest Science, Kangwon National University, Chuncheon 24341, Republic of Korea.
E-mail address: ktlim@kangwon.ac.kr (K.-T. Lim).

https://doi.org/10.1016/j.mtcomm.2022.103906
Received 12 January 2022; Received in revised form 22 June 2022; Accepted 24 June 2022
Available online 27 June 2022

and biocompatibility. Their structure resembles a self-adhesive mussel protein, and they exhibit strong adhesive properties with different organic and inorganic substrates through covalent or non-covalent interactions with the surfaces. Compared to the pure polymer hydrogel, a significant enhancement in adhesiveness was observed in the PDA-incorporated hydrogels [16,17]. PDA is widely used in cancer treatment, shape memory, and self-healing. It absorbs NIR light and effectively transfers thermal energy [18]. Under NIR light irradiation, enhanced self-healing and shape-memory properties were observed in PDA-incorporated PVA hydrogels [19]. Carbon nanomaterials, including carbon quantum dots, carbon nanotubes, and graphene, have been widely used as reinforcing and conductive agents in polymer matrices, due to their superior physiochemical properties, such as high surface area, enhanced mechanical and thermal strength, superior electrical and thermal conductivity and biocompatibility [20]. The carbon nanomaterials derived from bio-waste resources have paid wide attention due to their easy availability and simple methodology. Different techniques, such as heat treatment and hydrothermal, are profoundly applied to synthesize carbon nanomaterials from biomass. Biomass materials, such as tea and rice residues, bagasse, and peanuts, are appropriate sources of carbon and are frequently utilized to prepare carbon nanomaterials [21,22]. The use of biomass to produce value-added materials can minimize the cost of raw materials and help in carbon recycling [23]. The biomass-derived carbon nanomaterials exhibited superior biocompatibility, and fluorescence properties, and explored in sensing, imaging, and other applications [24]. The strain sensing ability of PVA, chitosan or modified chitosan, sodium alginate, and β-cyclodextrin with different nanomaterials, such as tannic acid and carbon nanotubes, have been reported earlier with good sensitivity [14,15,20,25–30]. The ions sensing and bio-imaging potentials of waste biomass-derived carbon nanomaterials have been widely studied [31]. However, the strain sensing potential of waste biomass-derived carbon nanomaterials is not yet fully explored. Furthermore, conductive hydrogels with antibacterial potential are highly desired to develop bionic skin, due to their bacteria inhibiting potential, which causes infections in contact with human body.

Herein, we demonstrated the strain sensing ability of PVA polymer hydrogels composed of cucumber peels-derived CDs and PDA. The CDs were prepared through a heat treatment process and characterized by different spectroscopic tools. The mechanical strength, viscoelastic properties, and recovery properties of the hydrogels were evaluated. The obtained hydrogels exhibited improved mechanical and recovery strength. The adhesiveness and NIR-responsiveness efficiencies of the hydrogels were also monitored. The presence of PDA@CDs endowed adhesiveness and conductivity into hydrogels. The developed hydrogels have no adverse effects on human dermal fibroblasts (HDFs) cells, indicating biocompatibility. Antibacterial efficacy of the developed hydrogels was monitored with *Escherichia coli.* The strain-sensing efficiency of the developed hydrogels was explored on different parts of the human body (finger, wrist, and knee joint). This study opens new opportunities to develop multipotential hydrogels using bio-waste-derived CDs for sensing applications.

2. Experimental section

2.1. Materials

The following chemicals were used as received without further purification: poly (vinyl alcohol) (PVA) (1500 MW, >99%, Daejung Chemicals, Gyeonggi-do, Republic of Korea), dopamine hydrochloride, 4, 6-diamino-2-phenylindole dihydrochloride (DAPI), paraformaldehyde (PFA), bovine serum albumin (BSA), (Sigma-Aldrich, St. Louis, USA), 1.5 M Tris-HCl buffer (pH-8.8, Bio-Rad), and F actin probe, and mounting media (Invitrogen, Thermo-Fischer Scientific, USA). Cucumber peels were collected from local markets.

2.2. Preparation of carbon dots (CDs)

The CDs were synthesized through heat treatment in an open atmosphere. The collected peels were heated at 230 °C for 2 h, followed by dispersion in ultrapure water. The dispersed solution was sonicated for 30 min and filtered, and the filtrate was centrifuged at 10,000 rpm for 15 min. The supernatant was collected and dialyzed with cellulose bags (MWCO: 12–14 kDa) against distilled water for 2 days. The dialyzed samples were concentrated using a rotary evaporator. After that, the sample was freeze-dried using a freeze-dryer (EYELA® Freeze Drying Unit 2200, Tokyo, Japan) for 48 h to obtain a dry sample.

2.3. Synthesis of polydopamine (PDA) functionalized CDs (PDA@CDs)

PDA@CDs were synthesized *via* the self-polymerization process of dopamine under alkaline conditions, as previously reported somewhere else [32]. In brief, 3 mg of CDs was re-suspended in 5 mL of distilled water, followed by adding dopamine hydrochloride (10 mL, 3 mg/mL) to the CDs solution. The required amounts of Tris buffer were added to the solution mixture to maintain the pH of 8.5 with continuous mechanical stirring for 24 h. The obtained sample was filtered to remove the unreacted chemical moieties, followed by the dialysis using a cellulose bag against distilled water for 3 days. The dialyzed sample was concentrated using a rotary evaporator, followed by freeze-drying using the freeze-dryer.

2.4. Synthesis of poly (vinyl) alcohol (PVA)/PDA@CDs hydrogels

The PVA hydrogel was prepared in the aqueous medium. For this, the required amount of PVA (12 *wt.* %) was added to distilled water and heated at 90 °C for 3 h to obtain a homogenous solution, followed by the addition of 0.1 M borax solution. The air bubbles were removed *via* the sonication process. After that, the sample was first stored at 4 °C for 10 h then at −20 °C for 4 h to obtain highly cross-linked hydrogel. The hydrogel was unfrozen at room temperature. PVA/PDA@CDs hydrogels were developed similarly by adding the required amounts of PDA@CDs (1, 2, and 4 *wt.* %, w.r.t. to PVA *wt.*) in the PVA matrix and stirring for 4 h to obtain a homogenous mixture. The cross-linking process in composite hydrogels was performed similarly with PVA hydrogel. The developed hydrogels were designated as PVA and PVA/PDA@CDs-x, where x is the amount of PDA@CDs in the PVA matrix.

2.5. Characterization of CDs, PDA@CDs, and PVA/PDA@CDs hydrogels

Fourier transform infrared (FTIR) spectroscopy (Frontier, Perkin Elmer, UK) was used to determine the functional groups in CDs, PDA@CDs, and the interaction between the PVA and PDA@CDs moieties in the wavelength range of 4000–500 cm^{-1} with a resolution of 4 cm^{-1}. The number of the scan was 64. The field emission transmission electron microscopy (FE-TEM) (JEM, 2100 F, Jeol, Japan) was used to measure the size and morphology of CDs. For this, a 5 μL aqueous suspension of CDs was drop-casted onto the carbon grid (200–300 square mesh) and allowed to dry for 5 h. After that, the morphologies were captured at a high operating voltage of 200 kV. Atomic force microscopy (AFM) (Nanoscope 5/multimode 8, Bruker, Germany) was utilized to examine the morphology of CDs and PDA@CDs. For this, 10 μL aqueous suspension of CDs was drop-casted onto the mica surface and allowed to dry for 6 h. After that, the morphologies were captured using the Nanoscope 5 instrument.

The X-ray diffractometer (XRD) (X′Pert PRO MPD, Philips, Eindhoven, Netherlands) was used to assess the structure of CDs at operating voltage and current of 40 kV and 40 mA, respectively, with Cu Kα radiation (λ = 1.5414 A°). The operating range (2θ) was 5–40°. The UV–visible spectrophotometer (Libra S80, Biochrom, UK) was used to know the electronic transition in CDs in the measured range of 200–800 nm with the scanning rate of 10 nm/min. Differential scanning

calorimetry (DSC, TA instruments) was performed to determine PDA@CDs effects on polymer melting behavior at 25–250 °C under a nitrogen atmosphere. The heating rate for DSC measurement was 10 °C/min. The mechanical strength of the developed hydrogels was determined by using the universal testing machine (UTM) (MCT-1150, A&D, Co. Japan) in compression mode with a compressive speed of 10 mm/min. The compressive modulus, compressive strength, and densification strain were calculated from the slope of the stress-strain curve in the elastic region, the stress value at the compressive yield point, and the strain value at the intersection point between the lines of stress plateau of the stress-strain curve, respectively. Each experiment was performed in triplicate ($n = 3$), and the data were reported as mean value ± standard deviations. The viscoelastic and recovery properties of the developed hydrogels were evaluated using an ARES-G2 rheometer (TA Instrument, New Castle, Delaware, USA) with a 6 mm parallel plate at 25 °C.

2.6. Macroscopic self-healing examination

The macroscopic self-healing potential of the synthesized hydrogels was assessed using the cut and join method. The hydrogel with the desired structure was cut and separated from its original structure. Subsequently, the separated structures were toughened, and the healing process was monitored at room temperature.

2.7. Adhesive measurement

For the adhesive analysis, 200 mg of the hydrogel was placed on a plastic surface and spread over an area of 25 mm × 15 mm. Subsequently, another plastic sheet with a similar dimension was kept over the hydrogel and left for 10 min. Uniaxial tensile measurements were conducted to assess the adhesive strength of the hydrogels. All measurements were performed in triplicate ($n = 3$), and the average data were taken.

2.8. Photo-thermal performance of hydrogels

The photo-thermal performance of the developed hydrogels was analyzed using an 808 nm NIR laser source (MDL-H-808 5 W). The hydrogels (200 mg) were placed in an Eppendorf tube and irradiated with the NIR laser density (I) at 0.5, 1.0, and 1.5 W/cm^2 for different period. The distance between the NIR laser source and the sample was 8 cm. The changes in the temperature and thermal images were recorded using a NIR thermal imager (FLIR, Sweden). All experiments were conducted in triplicate ($n = 3$), and the results are presented as mean ± standard deviations.

2.9. Shape memory analysis

The shape memory potential of the developed hydrogels was determined by the cyclic bending method, as shown previously elsewhere [33]. The hydrogels with definite dimensions were deformed at a particular angle (θ_i), and kept in hot water at 55 °C for 10 s. After that, the deformed hydrogels were transferred to normal water at 25 °C for 30 s to obtain the properly deformed hydrogels (θ_f). The shape fixing ratio (R_f) of the hydrogels was measured by using the given formula,

$$Shape\quad fixing\quad ratio\quad (R_f) = \frac{\theta_f}{\theta_i} \times 100$$

The shape recovery ability of the hydrogels was examined by again placing the de-formed hydrogels in hot water at 55 °C for 10 s, followed by measuring the residual angle (θ_p). The shape recovery ratio (R_r) of the de-formed hydrogels was calculated by using the equation given below,

$$Shape\quad recovey\quad ratio\quad (R_r) = \frac{\theta_f - \theta_p}{\theta_f} \times 100$$

2.10. Cytotoxicity of the hydrogels

Cytotoxicity of the synthesized hydrogels was examined in the presence of human dermal fibroblasts (HDFs) cells through WST-8 assay. Briefly, 1×10^4 cells were cultured with or without hydrogels in a 5% CO_2 incubator at 37 °C for 24 and 72 h. The cultured groups without hydrogel treatment were taken as control. After incubation, cells were washed with PBS (2 times), and 100 μL of fresh cultured media were in cultured cells. After that, 10 μL WST-8 dye were added to cultured cells and further incubated for 2 h to form the formazan. The absorbance at 450 nm was recorded using a spectrophotometer (Infinite® M Nano 200 Pro, TECAN, Switzerland) to quantify the developed formazan. All experiments were conducted in triplicate ($n = 3$), and the results are given as mean optical density (OD) ± standard deviations (SDs). Statistical significance was considered as * $p < 0.05$.

The HDFs morphologies were recorded using an inverted fluorescence microscope (DMi8 Series, Leica Microsystems, Germany) after 24 h of treatment. In brief, 2.0×10^4 cells were incubated with or without hydrogels. The groups without hydrogel treatment were considered as control. After that, cells were washed with PBS (2 times) and fixed with a 4% PFA solution. The fixed cells were again washed with PBS (2 times) and treated with 0.1% Triton-X 100 for 10 min, followed by 1% BSA treatment for 60 min. After that, cells were incubated with 200 μL of Alexa flor 488-conjugated Phalloidin for 20 min, and DAPI for 5 min. The excess stains were eliminated by washing with PBS (3 times). One drop of Prolong® Antifade mounting media was added, and morphologies were captured using a fluorescence microscope.

2.11. Evaluation of antibacterial potential

The antibacterial efficacy of the prepared hydrogels was assessed with *Escherichia coli* by agar diffusion assay method as earlier reported somewhere else [34]. Briefly, the new bacteria colonies were produced by suspending the few colonies of *Escherichia coli* in the nutrient broth and incubated at 37 °C for 12 h with stirring (200 rpm). The optical density (O.D.) of the newly produced bacterial was recorded at 600 nm through a spectrophotometer. The concentration of the newly generated bacteria was diluted by 10^{-2} orders from their initial concentrations. After that, the diluted bacteria were diffused on agar plates, followed by the addition of equal weights of the prepared hydrogels (0.10 g) on agar plates. The agar plates were incubated at 37 °C for different period (24, and 72 h). The experiments were accomplished in triplicate ($n = 3$).

2.12. Conductivity and sensing potential of hydrogels

The hydrogel conductivity was assessed using a four-probe instrument (MS Tech, Solution) connected to the Keithley 2460 source meter® at room temperature. The details of hydrogel dimensions and their resistance are given in Supplementary Table 1. The conductivity of hydrogels is calculated by using following equation.

$$\text{Conductivity} = \frac{L}{RA}$$

where, L, R, and A are the length, resistance, and area of the hydrogel, respectively.

The cyclic voltammetry (CV) behavior of the hydrogel was examined by using two electrodes in the sulfuric acid solution (1 mol/L) with the Keithley 2460 source meter® at room temperature. The platinum (Pt) disc and silver (Ag/AgCl) was used as working and reference electrodes, respectively. The potassium chloride (3.0 M) solution was used as a supporting electrolyte. The sensing potential of the developed hydrogels was examined using a Keithley 2460 source meter® at a constant voltage of 5 V. The length and diameter of the hydrogels were 24.5 mm and 7.44 mm, respectively. The change in the hydrogel current was

measured with time. The change in the relative resistance ($\Delta R/R_0$) was determined by using the following equation,

$$Relative\quad resistance\quad change\quad \left(\frac{\Delta R}{R_0}\right)(\%) = \frac{(R_s - R_0)}{R_0} \times 100$$

where, R_0, and R_s are the resistance of hydrogels before and after strain, respectively.

Strain sensitivity of the developed hydrogel was determined by gauge factor (GF), which was calculated by using following equation,

$$Gause\quad factor\quad (GF) = \frac{\left(\frac{\Delta R}{R_0}\right)}{\varepsilon}$$

where, ε is the applied strain.

2.13. Statistical analysis

Statistical analyses were performed with one-way ANOVA using Origin Pro9.0 software. Statistical significance was considered at $^{*}p < 0.05$, $^{**}p < 0.01$, and $^{***}p < 0.001$. All comparisons were made between the control and experimental groups. All experiments were performed in triplicate ($n = 3$), and the results are presented as mean ± standard deviations (SDs).

3. Results and discussion

3.1. Structural properties of CDs

A schematic representation of the synthesis of the multifunctional fluorescent hydrogel is presented in Scheme 1. The morphology of the cucumber peel-derived CDs was examined using TEM, and the image is shown in (Fig. 1a). The synthesized CDs exhibited a sheet-like morphology with an average diameter of 18 nm. The size distribution of CDs was measured using the particle size analyzer, and the obtained data is shown in (Fig. S1a). The average hydrodynamic size of the particles was detected to be 198.8 nm. The FTIR spectrum of the synthesized CDs is presented in (Fig. 1b). The FTIR spectrum shows several absorption peaks, suggesting the presence of different functional groups. The appearance of the absorption peaks at 3276, 1589, and 1064 cm^{-1} is ascribed to the hydroxyl (–OH stretching), carbonyl (–C═O vibration), and –C-O functional groups [35]. The absorption peaks at 2929 and

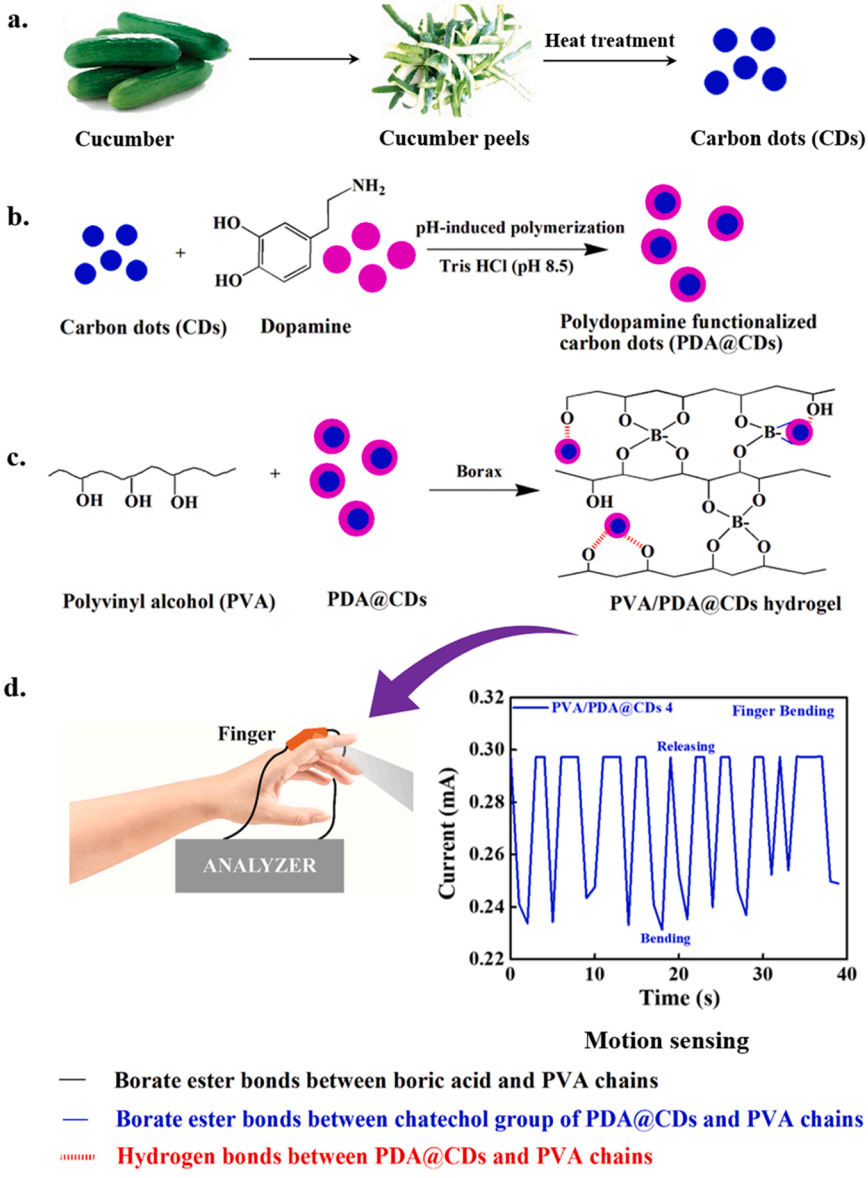

Scheme 1. Schematic presentation for the synthesis of hydrogels and their sensing applications. (a) Synthesis of carbon dots (CDs) from waste cucumber peels through heat treatment, (b) Functionalization of polydopamine (PDA) with the synthesized CDs through *in-situ* polymerization technique under alkaline conditions, (c) Fabrication of the chemically cross-linked polyvinyl alcohol/ polydopamine@carbon dots (PVA/PDA@CDs) hydrogels (possible interactions are mentioned below), and (d) Demonstration of the sensing application of the developed hydrogel.

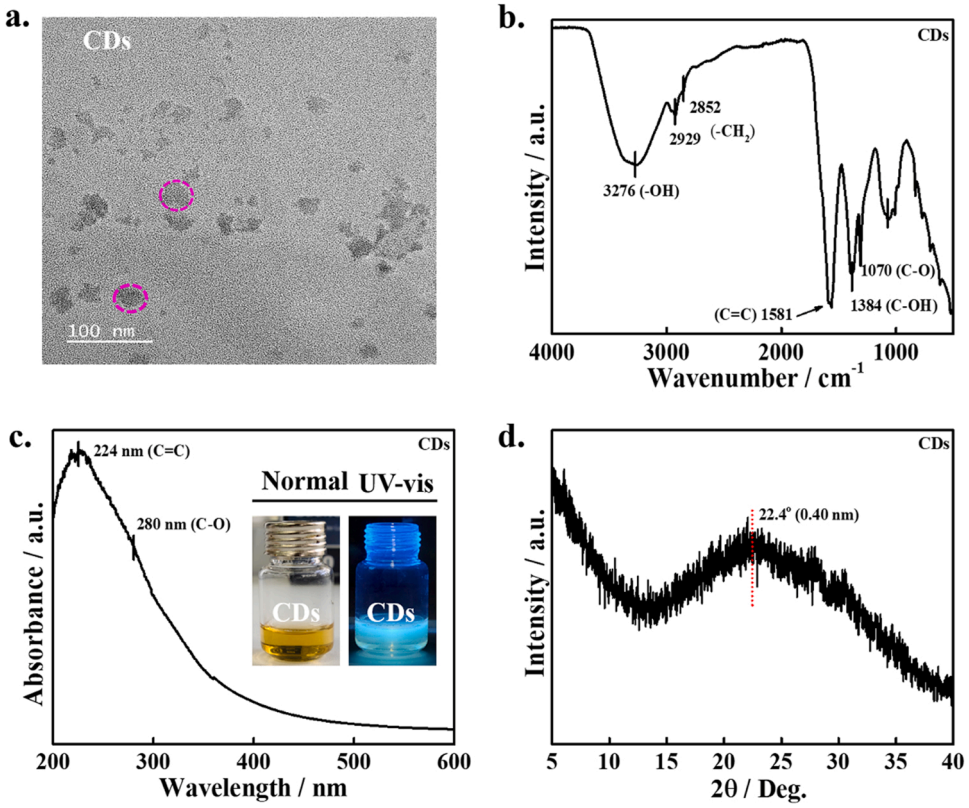

Fig. 1. Spectroscopic characterizations of the synthesized CDs. (a) TEM image of the synthesized CDs, (b) FTIR spectrum of CDs, (c) UV–visible spectrum (inset fluorescence color), and (d) XRD pattern of CDs.

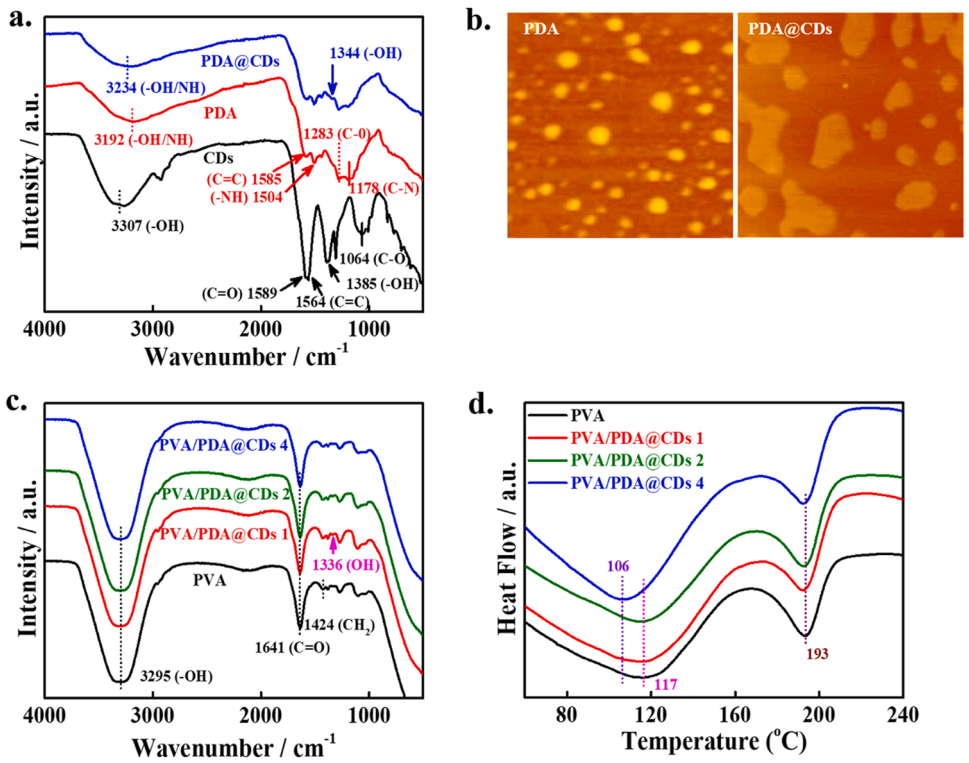

Fig. 2. Spectroscopic characterizations of PDA functionalized CDs. (a) FTIR spectra of the CDs, PDA, and PDA@CDs, (b) AFM images of PDA and PDA@CDs (1 μm × 1 μm), (c) FTIR spectra of the developed hydrogels, and (d) DSC curves of the developed hydrogels.

2852 cm^{-1} are associated with the stretching vibration of the $–CH_2$ group. The appearance of different C–O vibrations, mainly epoxy and hydroxyl, occurs in the region of 1384 – 823 cm^{-1}, and distinct absorption peaks are observed at 1384, 1308, 1070, 1009, and 823 cm^{-1} [36]. We further measured the UV–visible spectrum to assess the molecular structure of the synthesized CDs, and the spectrum is shown in (Fig. 1c). The spectrum exhibits an intense and a shoulder peaks at 224 and 280 nm, which are attributed to the $\pi \rightarrow \pi^*$ transition of C═C and the $n \rightarrow \pi^*$ transition of carbonyl groups (C═O), respectively [37]. The UV–visible spectrum confirmed the existence of different functional groups in the synthesized CDs. The fluorescence behavior of the synthesized CDs was examined under UV light (365 nm), and the images are shown in the inset of (Fig. 1c). No fluorescence behavior was detected under normal light, whereas a bright blue color was observed under UV light, indicating the fluorescence property of CDs. The fluorescence property of the synthesized CDs is attributed to the transition of electrons from one state to other states under UV irradiation. The structural properties of the synthesized CDs were evaluated by XRD analysis, and the obtained pattern is presented in (Fig. 1d). The CDs exhibit a broad diffraction peak at 22.4° with the corresponding D-spacing of 0.40 nm, suggesting the existence of a graphitic structure in the synthesized CDs. It is well-established that pure graphite exhibits a diffraction peak at 26.4° with a corresponding D-spacing of 0.34 nm [38]. However, the synthesized CDs demonstrate a higher D-spacing than pure graphite, suggesting the insertion of some functional groups inside the CDs layer.

3.2. Structural properties of PDA@CDs and developed hydrogels

The functionalization of CDs with PDA was performed *via* the *in-situ* polymerization process of dopamine under alkaline conditions. The FTIR spectra of the pure PDA and functionalized PDA (PDA@CDs) are shown in (Fig. 2a). The appearance of a broad absorption in PDA at 3192 cm^{-1} indicates the presence of amine ($–NH_2$) functional groups in the structure, which overlaps with the stretching vibration of hydroxyl groups (–OH) [39]. The absorption peaks at 1585 and 1504 cm^{-1} are ascribed to the C═C of the aromatic structure and bending vibration of the –NH groups, respectively. The absorption peak at 1178 cm^{-1} in PDA shows the presence of C–N functional groups, which originated from the indole ring of PDA. The PDA@CDs exhibit all the characteristic absorption peaks of PDA. However, a significant shift in the absorption peak of –NH/OH (3192 → 3234 cm^{-1}) was observed in PDA@CDs, suggesting a strong interaction between the PDA and CDs during the *in-situ* polymerization. The hydrogen bonding is the presumably primary interaction among the hydroxyl/amine groups of dopamine and oxygen-containing CDs [40]. Furthermore, a decrease in the intensity of the –OH absorption peak of CDs was observed in PDA@CDs, which is attributed to the bonding between the CDs and PDA hydroxyl groups. These findings indicate the successful functionalization of PDA with CDs during *in-situ* polymerization.

We examined the morphological changes in PDA and PDA@CDs using AFM, and the images are shown in (Fig. 2b). The pure PDA exhibited a nearly spherical morphology with an average diameter of 72.5 nm. In contrast, an increase in the diameter was observed in PDA@CDs, suggesting the wrapping of the PDA chain over CDs. The average diameter of the PDA@CDs was 90.6 nm. We further examined the retention of the fluorescence behavior of CDs in the PVA/PDA@CDs hydrogels, and the images under normal light and UV–visible light are shown in (Fig. S1b). No color was detected under normal light conditions, whereas a strong blue emission was observed under UV light (365 nm) irradiation, indicating that the hydrogel retained the fluorescence property of the synthesized CDs. Fluorescent hydrogels have broad applications in soft robotics and biological sensors [41]. FTIR spectra were recorded to assess the interaction between the PVA polymer chains and the incorporated PDA@CDs under gel conditions, and the results are presented in (Fig. 2c). The pure polymer and its composite hydrogels exhibit a broad absorption peak at 3295 cm^{-1}, which is assigned to the stretching vibration of the hydroxyl groups of PVA and PDA@CDs. The broad peak is due to the overlapping of hydroxyl groups in the gel conditions. The absorption peaks at 1641, and 1424 cm^{-1} in the hydrogels are assigned to the acetyl group (C═O) and bending vibration of methylene (CH_2), respectively [42]. Additionally, a new peak was observed in the composite hydrogels at 1336 cm^{-1}, which can be ascribed to the bending vibration of the hydroxyl group (–OH) of PDA@CDs. These results indicate that PDA@CDs were well dispersed and interacted with the PVA polymer chains. The borate ester and hydrogen bonding are the presumably key interaction among the oxygen-containing groups of PVA and the incorporated PDA@CDs. We further examined the effects of PDA@CDs on the melting behavior of the PVA hydrogels without using the cross-linking agent through the DSC measurement, and the results are shown in (Fig. 2d). The pure PVA hydrogel exhibits two endothermic peaks at 117 °C and 193 °C, attributed to the β_c relaxation of PVA crystalline regions and the melting of the crystalline domains [43]. The addition of PDA@CDs caused the lowering of the β_c relaxation temperature (117 °C → 106 °C), indicating more relaxation in the crystalline structures, leading to more stretchable orientations. However, no significant changes in the melting temperature of the crystalline domains were observed, suggesting that the distribution of PVA@CDs predominantly occurred within the β_c structures.

3.3. Mechanical and viscoelastic behavior of hydrogels

The mechanical strength of the developed hydrogels was assessed by using UTM in compressive mode, and the obtained stress-strain curves are presented in (Fig. 3a). The compressive modulus, compressive strength, and densification strain values were determined from the stress-strain and values are given in Table 1. The developed hydrogels show a typical compressive behavior of porous materials, including the linear elastic region at low-stress values, followed by the plateau and densification regions with significant enhancement in compressive stress. The composite hydrogels exhibited improved mechanical strength and stiffness than the pure polymer hydrogel and further increased with increasing PDA@CDs contents in the polymer matrix, demonstrating the reinforcing effect of PDA@CDs, due to better interactions between polymer chains and PDA@CDs [44]. The composite hydrogels showed a lower densification value than pure polymer hydrogels. The decrease in densification value can be attributed to the decrease in the porosity of the scaffolds.

The rheological behavior of the developed hydrogels was measured using a rheometer in the angular frequency (ω) ranges of 0.1–100 rad/s. The change in the storage modulus (G′, solid line) and loss modulus (G″, without line) in the measured regions is shown in (Fig. 3b). The composite hydrogels exhibit a greater storage modulus than the pure polymer hydrogel, which was further increased by increasing the PDA@CDs content in the PVA matrix, demonstrating the reinforcing effects of the incorporated PDA@CDs. Approximately 3.5 times ($1.37 \times 10^4 \rightarrow 4.62 \times 10^4$ Pa) enhancement in the storage modulus was observed in the composite hydrogels than in pure polymer hydrogels. The enhancement in the storage modulus reflects the solid-like properties in the hydrogels through the greater interactions between the crosslinking agent and the functional groups of the PVA and PDA@CDs. Three kinds of interaction are possible between the PVA, PDA@CDs, and cross-linking borax. Borate ester bonds between the hydroxyl groups of PVA chains and boric acid; borate ester bonds among hydroxyl groups of PVA chains, and catechol groups of PDA@CDs; and hydrogen bonding between the hydroxyl groups of PVA chains, and catechol groups of PDA@CDs are the possible primary interactions in the hydrogel components [45]. At higher frequencies, the elasticity becomes more prominent due to the greater entanglement of the polymer chains. An enhancement in the storage modulus of PVA hydrogels was reported with cellulose nanocrystals (CNCs) cross-linked with borax [46]. The composite hydrogels exhibit higher loss moduli than that of the pure polymer hydrogel. However, their magnitudes are lower than those of the storage moduli,

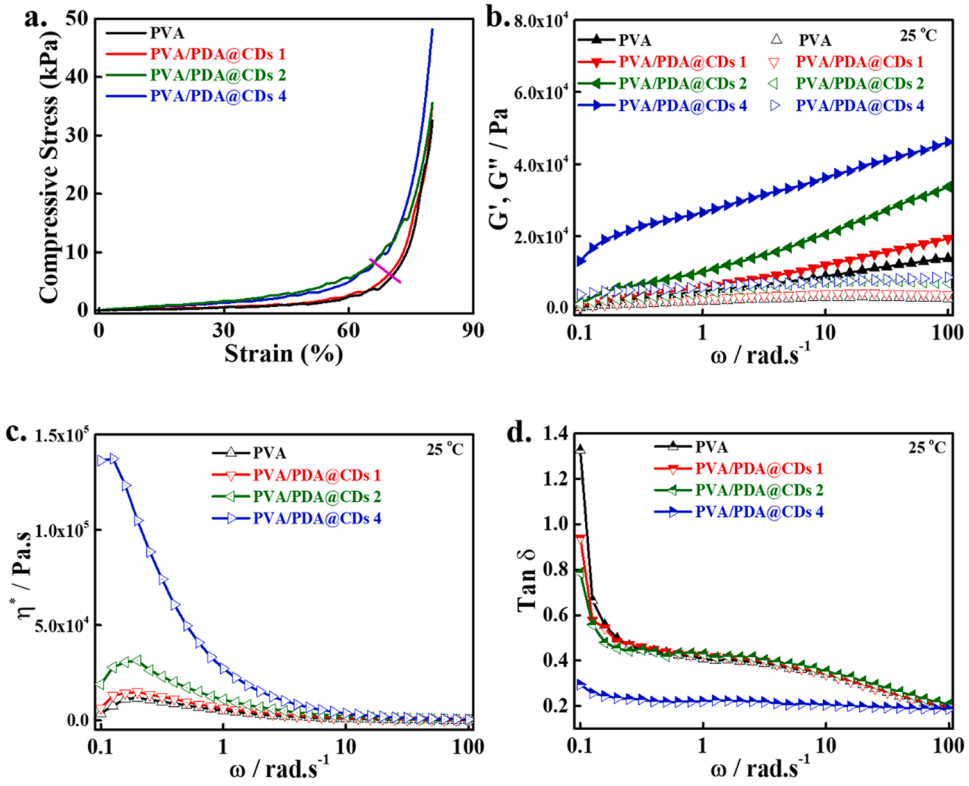

Fig. 3. Mechanical and viscoelastic evaluation of the developed hydrogels. (a) Stress-strain curves of the developed hydrogen under compressive mode, (b) Storage and loss moduli of the developed hydrogels, (c) Corresponding complex viscosity of the hydrogels, (d) Measurement of damping factor of the indicated hydrogels in the measured regions.

Table 1
Mechanical properties of the developed hydrogels.

Sample	Compressive modulus (kPa)	Compressive strength (kPa)	Densification strain (%)
PVA	0.017 ± 0.003	32.41 ± 0.4	70.75 ± 1.01
PVA/ PDA@CDs 1	0.019 ± 0.004	34.93 ± 0.3	69.48 ± 0.08
PVA/ PDA@CDs 2	0.042 ± 0.004	35.56 ± 0.2	66.39 ± 1.1
PVA/ PDA@CDs 4	0.043 ± 0.003	48.13 ± 0.4	66.16 ± 1.01

indicating that the viscoelasticity of the developed hydrogels is defined by elastic characteristics.

The changes in the viscosity complex (η *) of the fabricated hydrogels in the measured angular frequency regions are shown in (Fig. 3c). The composite hydrogels demonstrated a greater η * value throughout the measured angular frequency regions than those of the pure polymer hydrogels, indicating a solid-like structure within the hydrogels, which became more prominent at higher PDA@CDs contents. A drastic decrease in η * ($1.36 \times 10^5 \rightarrow 4.69 \times 10^2$ Pa.s) occurred at higher angular frequency regions, indicating the fluid characteristics of the hydrogels. This decrease in the η * value can be attributed to the destruction of the ordered structures at the higher angular frequency, resulting in a lower η * value. This finding suggests that the developed hydrogels have viscoelastic characteristics. The change in the damping factor (tan δ) of the developed hydrogels throughout the measured regions is shown in (Fig. 3d). The damping factor provides valuable information regarding the internal structure of the materials. The material with a lower damping factor exhibits greater solid-like properties than those with a higher damping factor [47]. Interestingly, the composite hydrogels had a lower damping factor than that of the pure polymer hydrogel, suggesting ordered structure through strong interactions. This value was further decreased by increasing PDA@CDs content in the PVA matrix, which facilitated the formation of more compact and oriented structures. These results suggest that the developed hydrogels have highly interactive and ordered structures, enhancing the physicochemical properties.

3.4. Self-healing and recovery potential of hydrogels

In strain sensing applications, self-healing materials have received considerable attention because of their attractive re-healing ability without involving external factors [48,49]. The reversible or dynamic interactions between the material components are responsible for the resumption of the initial structure and physicochemical properties [50]. Here, we examined the macroscopic self-healing potential of the developed hydrogel by cutting and re-joining the separated parts at room temperature, and the representative images are shown in (Fig. 4a). A definite size of hydrogel was taken and separated into two parts, followed by the coloring of one part with the Coomassie blue dye solution to visualize the self-healing process. The separated hydrogels were toughed with each other, and their re-joining ability was monitored. The separated hydrogels were completely united within 1 h at room temperature, showing their self-healing properties. A possible mechanism for breaking and re-joining the hydrogel components is shown in (Fig. 4b). The breaking of the borate esters between PVA chains and boric acid, catechol groups of PDA and boric acid, and hydrogen bonds among PVA chains and PDA@CDs occurs during exposure to external stress. These interactions are reversible and re-formed after toughing the separated parts of the hydrogel.

We examined the quantitative recovery efficiency of the developed hydrogels by measuring the viscosity change under different shear

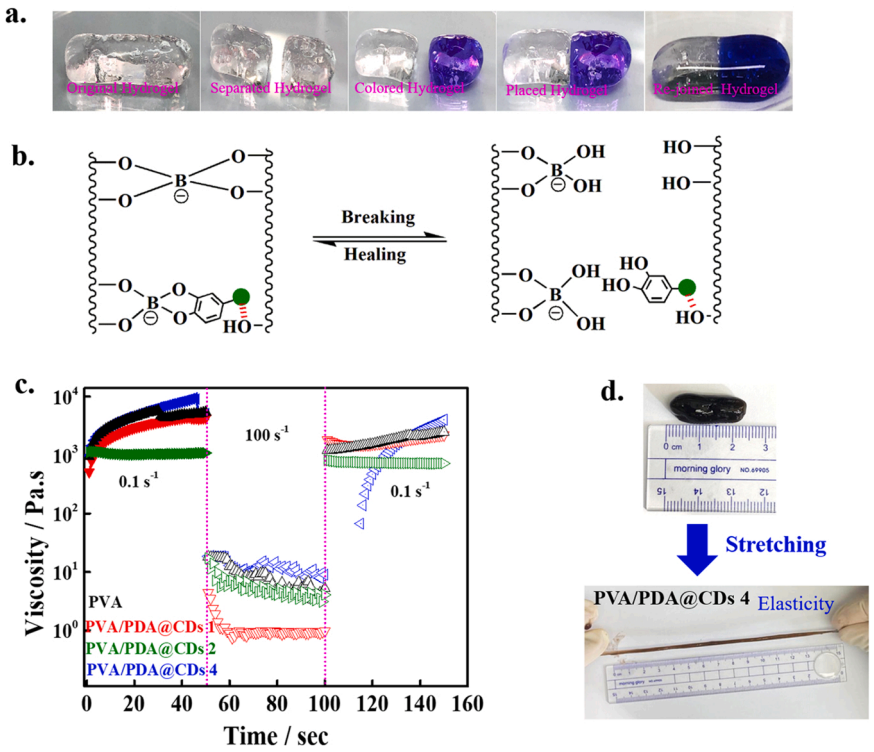

Fig. 4. Examination of the self-healing potential of the developed hydrogel. (a) Macroscopic self-healing behavior of the developed hydrogel, (b) Possible mechanism for self-healing in the developed hydrogels, (c) Recovery strength of the developed hydrogels, and (d) Stretchability test of the developed hydrogel.

conditions. Initially, a slow shear rate (0.1 s^{-1}) was applied for 50 s, followed by implementing a high shear rate (100 s^{-1}) for 50 s, and a change in the viscosity was measured. The high shear rate was applied to destroy different interactions in the hydrogels. After that, the shear rate suddenly dropped to 0.1 s^{-1} for 50 s. The changes in the viscosity of the developed hydrogels under different shear rate conditions are shown in (Fig. 4c). The viscosity of PVA, PVA/PDA@CDs 1, PVA/PDA@CDs 2, and PVA/PDA@CDs 4 after 50 s of 0.1 s^{-1} shear rate was 5412.19, 4319.35, 1083.76, and 5027.79 Pa.s, which further decreased to 5.1831, 0.9696, 4.0540, and 8.8989 Pa.s under 100 s^{-1} shear rate, respectively. The viscosity was again increased by implementing of a 0.1 s^{-1} shear rate. The final viscosity was 2472.37, 2207.12, 719.16, and 4015.63, Pa. s for PVA, PVA/PDA@CDs 1, PVA/PDA@CDs 2, and PVA/PDA@CDs 4, respectively. The recovery values were calculated and found to be 45.58%, 51.07%, 65.98%, and 79.69% for PVA, PVA/PDA@CDs 1, PVA/PDA@CDs 2, and PVA/PDA@CDs 4 hydrogels, respectively. A sudden decrease in the hydrogel viscosity at a higher shear rate is attributed to the relaxation of polymer chains, which leads to minimizing the interactions between the hydrogel components and enhancing the fluid characteristics. The enhancement in the viscosity of the hydrogels was observed at a low shear rate, suggesting the rebuilding of the solid-like properties through strong interactions among the hydrogel components. The improvement in the recovery strength of nanocellulose-based hydrogels was also reported by creating solid-like characteristics *via* different interactions [51].

We further assessed the elasticity and flexibility potentials of the developed hydrogels by the stretching process, and the images of the hydrogel before and after stretching are presented in (Fig. 4d). Stretchability and flexibility are crucial properties required for strain-sensing applications. Brittle materials are not suitable for strain-sensing applications due to the destruction of the structure under applied stress [52]. Actuators made of flexible and stretchable materials are more compatible with human tissues than their solid equivalents. Here, we show the images of PVA/PDA@CDs 4 hydrogels before and after stretching. A stretchability of approximately 650% was observed in the developed hydrogel. Furthermore, the stretched hydrogels were bent and stretched without breaking, demonstrating their flexibility potential. Furthermore, the developed hydrogels can be easily molded in the desired shape, showing their moldability ability. The stretchability potential of the developed hydrogel was also confirmed through UTM in elongation mode (10 mm/min), and the result for PVA/PDA@CDs-4 hydrogel is shown in (Fig. S2). The hydrogel exhibited superior elongation property, showing its stretchability potential.

3.5. *Adhesive potential of hydrogels*

The adhesiveness ability of the hydrogels was examined with different surfaces, including human finger, 3D-printed polymer (vinyl acrylate), glass, and empty and water-filled centrifuge tubes, and the adhered images are shown in (Fig. 5a). The polymers were strongly adhered to different surfaces, demonstrating their adhesiveness potential. Interestingly, the developed hydrogel was tightly adhered with a filled centrifuge tube (45 mL, water) because of the strong interactions between the hydrogel and tube layer. Adhesiveness is an important property required for wearable electronic devices and sensing applications. This property provides an attractive and alternative approach for strain-sensing applications without using external tape or binders, which may have adverse effects on the epidermis layers of the skin and cause pain during peel-off due to the high binding strength of tapes or binders [53,54]. A possible mechanism for the adhesion of the developed hydrogel with a glass surface is shown in (Fig. 5b). The interaction between the active functional groups of the glass surface and hydrogel components is responsible for adhesiveness. The glass contains charged silicate groups in its structure, which strongly interact with the active groups of the hydrogel components and cause adhesiveness. In a 3D-printed polymer structure, charged acrylates are present, strongly binding with the hydrogel components. We conducted a lap shear test with plastic surfaces to measure the quantitative adhesiveness efficiency of the developed hydrogels after 10 min of treatment. The displacement *versus* load curves for the adhesive strength measurement is shown in

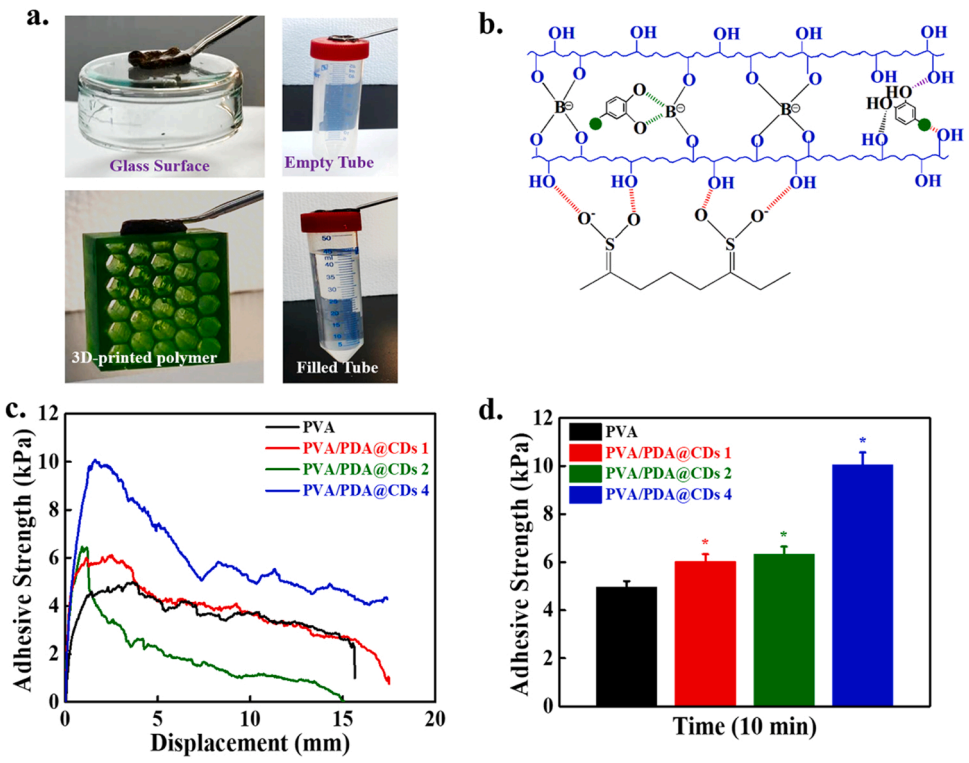

Fig. 5. Evaluation of the adhesive potential of the developed hydrogels. (a) Adhered hydrogels with different surfaces, (b) Possible mechanism for adhesion with glass surface, (c) Adhesive strength *vs* displacement curves, and (d) Quantitative values of the adhesive strength.

(Fig. S3). The adhesive strength *versus* displacement curves of the developed hydrogels is presented in (Fig. 5c). Compared with the pure polymer hydrogel, an improvement in adhesiveness occurred in the composite hydrogels, exhibiting superior adhesive potential. This tendency was further enhanced with increasing PDA@CDs content in the polymer matrix owing to the strong interactions with hydrogels and

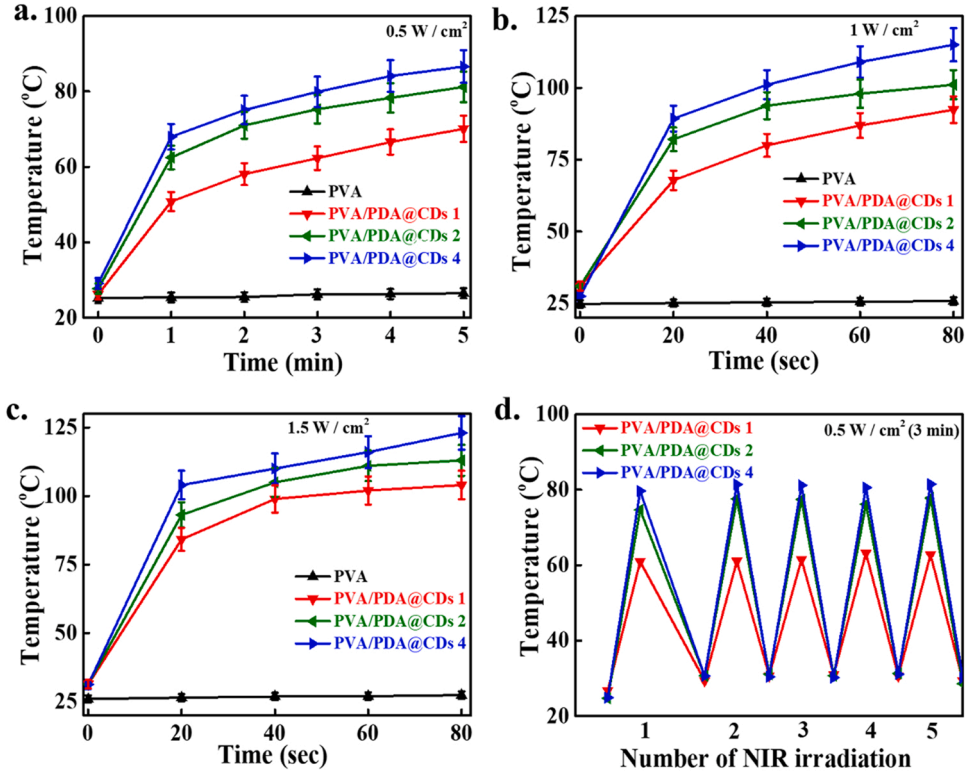

Fig. 6. NIR response of the developed hydrogels. (a) With 0.5 W cm^{-2}, (b) 1 W cm^{-2}, (c) 1.5 W cm^{-2} laser power for indicated period, and (d) Stability of the developed hydrogels under different cycles.

applied surfaces.

PDA has self-adhesive and biocompatible properties. CDs can also facilitate adhesiveness with other substrates *via* π–π or hydrophobic interactions. Hence, it is anticipated that the incorporation of functionalized PDA@CDs would increase the adhesiveness and allow applications in epidermal-based strain sensing [55]. The adhesive properties of the materials are profoundly affected by their components, applied surfaces, and adhesion time [56]. The quantitative values of the adhesive strength of the hydrogels are given in (Fig. 5d). The adhesive strength was 4.96, 6.03, 6.33, and 10.06 kPa for PVA, PVA/PDA@CDs 1, PVA/PDA@CDs 2, and PVA/PDA@CDs 4, respectively. The human skin has amine and carboxylic functional groups. Therefore, the developed hydrogels are expected to firmly adhere to the human skin through different interactions [57].

3.6. NIR responsiveness of hydrogels

Stimuli-responsive hydrogels are considered smart materials and have received considerable attention in soft robotics, wearable electronic devices, and sensors. Different stimuli, including light, temperature, pH, and magnetic and electric fields, have been widely applied to observe the response of these materials. NIR light is considered a suitable stimulus source because of its remote and precise response performance [58]. It is well-known that the conductive polymers or nanomaterials, like polypyrrole, PDA, or CDs, have the potential to absorb NIR light and convert them into heat. Therefore, it is anticipated that the hydrogels made of these materials could also demonstrate photo-thermal properties. We measured the NIR responsiveness of the developed hydrogels at different power intensities of laser light (0.5, 1, and 1.5 W/cm^2) for different periods, and the results are shown in (Fig. 6). The change in the hydrogels temperature irradiated at 0.5 W/cm^2 laser intensity for 5 min is shown in (Fig. 6a). Compared to that of the pure polymer hydrogel, a rapid enhancement in the temperature was observed in the composite hydrogels, revealing their NIR-responsive potential. This enhancement in the temperature of the composite hydrogels is attributed to the cumulative effects of PDA and CDs in the polymer matrix, which is highly active toward NIR light and effectively transforms light to heat [59]. The hydrogel with a higher content of PDA@CDs exhibited greater enhancement in temperature due to the enhanced conversion of light to heat by PDA@CDs. The changes in temperature of the hydrogels at 1.0 and 1.5 W/cm^2 laser irradiation are shown in (Fig. 6b and c). The change in the hydrogel temperature at the higher power intensity (1.0 and 1.5 W/cm^2) followed similar patterns as irradiated at a low power intensity (0.5 W/cm^2). However, the magnitude of the temperature change was high at higher power intensity than low power intensity. The PVA/PDA@CDs 4 hydrogel exhibited a higher change in the temperature than other hydrogels at a fixed intensity of laser light. This enhancement in the temperature can be assigned to the greater conversion of light into heat by higher amounts of PDA@CDs in the polymer matrix.

However, no significant change in the pure polymer hydrogel temperature was noticed under different conditions, suggesting its passiveness towards NIR light. The thermal images of the NIR laser-irradiated hydrogels are shown in (Fig. S4). We further performed the NIR responsiveness of the developed hydrogels at (0.5 W/cm^2, 3 min) for five cycles to examine their cyclic performances, and the results are shown in (Fig. 6d). The hydrogels exhibited a nearly identical change in the temperature after five cycles of NIR irradiation, demonstrating that the hydrogels maintained their photo-thermal properties after different cycles. These results indicate that the developed hydrogels have significant photo-thermal conversion potential, which can be explored for different applications. Xiao and coworkers reported the healing effect of NIR light in electro-conductive hydrogels for wearable strain sensors. The NIR irradiated hydrogels were rapidly healed and showed strain sensing potential with good sensitivity [60].

3.7. Shape memory behavior of hydrogel

The temperature-assisted shape memory ability of the developed hydrogels was examined to assess their shape retention and recovery potential, and the images are shown in (Fig. 7a). The obtained images indicate that the hydrogels can easily deform at the given temperature (55 °C) within 10 s and retain their temporary structure at 25 °C, demonstrating their shape fixation potential. The shape fixation ability in the developed hydrogels can be assigned to the destruction in the interactions within hydrogel components due to the motion of the polymer chains at a higher temperature and immediately cross-linked at a low temperature, causing the shape fixation ability. The PDA@CDs incorporated hydrogels exhibited better shape fixation potential than the pure polymer and increased with increasing PDA@CDs contents in the polymer matrix. The better shape fixation ability of the composite hydrogels is attributed to the greater extent of destruction in interactions at a high temperature and a high cross-linking ability in the hydrogels at a low temperature.

Furthermore, the de-formed hydrogels recovered their original structure, showing their shape memory ability. The destruction of the temporary structure can explain the origin of the shape memory potential in the developed hydrogels, and the re-orientation of the polymer chains with better interactions led to the shape memory potential. The rheological analysis (change in the viscosity) at different shear rates indicated the re-organization of the polymer chains in the developed hydrogels (Fig. 4c). The composite hydrogels demonstrated improved shape recovery ability than the pure polymer hydrogel and further increased with PDA@CDs contents in the polymer matrix. The improved shape recovery potential in the composite hydrogels is assigned to the greater destruction of the temporary structure and re-organization of the polymer networks, leading to a more organized structure.

The quantitative value of shape fixation is shown in (Fig. 7b). The shape fixation value was 88.9%, 94.72%, 95.61%, and 97.26% for PVA, PVA/PDA@CDs 1, PVA/PDA@CDs 2, and PVA/PDA@CDs 4, respectively. The enhancement in the shape fixation ability in the composite hydrogels can be assigned to a greater extent of destruction in the interactions due to the deformation of polymer chains with an external stimulus and formed a temporary cross-linked structure after the removal of the stimulus. The quantitative shape recovery value of the developed hydrogels is given in (Fig. 7c). The shape recovery was 71.14%, 88.91%, 91.99%, and 94.15% for PVA, PVA/PDA@CDs 1, PVA/PDA@CDs 2, and PVA/PDA@CDs 4, respectively. The higher shape recovery value of the composite hydrogels can be attributed to the better re-organization of the polymer networks through interactions. The possible mechanism for shape fixation and recovery in the developed hydrogels is presented in (Fig. 7d). When the hydrogel is subjected to a particular shape, re-structuring occurs with external stress. In the presence of the external stimulus, the de-formed polymer chains formed a temporary cross-linked structure. The composite hydrogels contain more active functional groups in their domains than the pure polymer hydrogel, and their number increased with increasing PDA@CDs contents. Therefore, there is a high opportunity for structural destruction with an external stimulus, and, subsequently, the formation of a temporary cross-linked structure. After removing the external stress, the polymer chains and PDA@CDs begin to relax, and disruption of the temporary structure occurs leading to the return to original state [61]. This result shows that the developed hydrogels have remarkable shape memory efficiency and can be utilized in soft robotics and sensing applications.

3.8. Cytotoxicity and antibacterial analysis

The cytotoxicity evaluation of the developed hydrogels is necessary to develop human motion sensing devices in wearable electronics. The cytotoxicity of the developed hydrogels was examined with HDFs cells after 24, and 72 h of incubation, and the results are shown in (Fig. 8a).

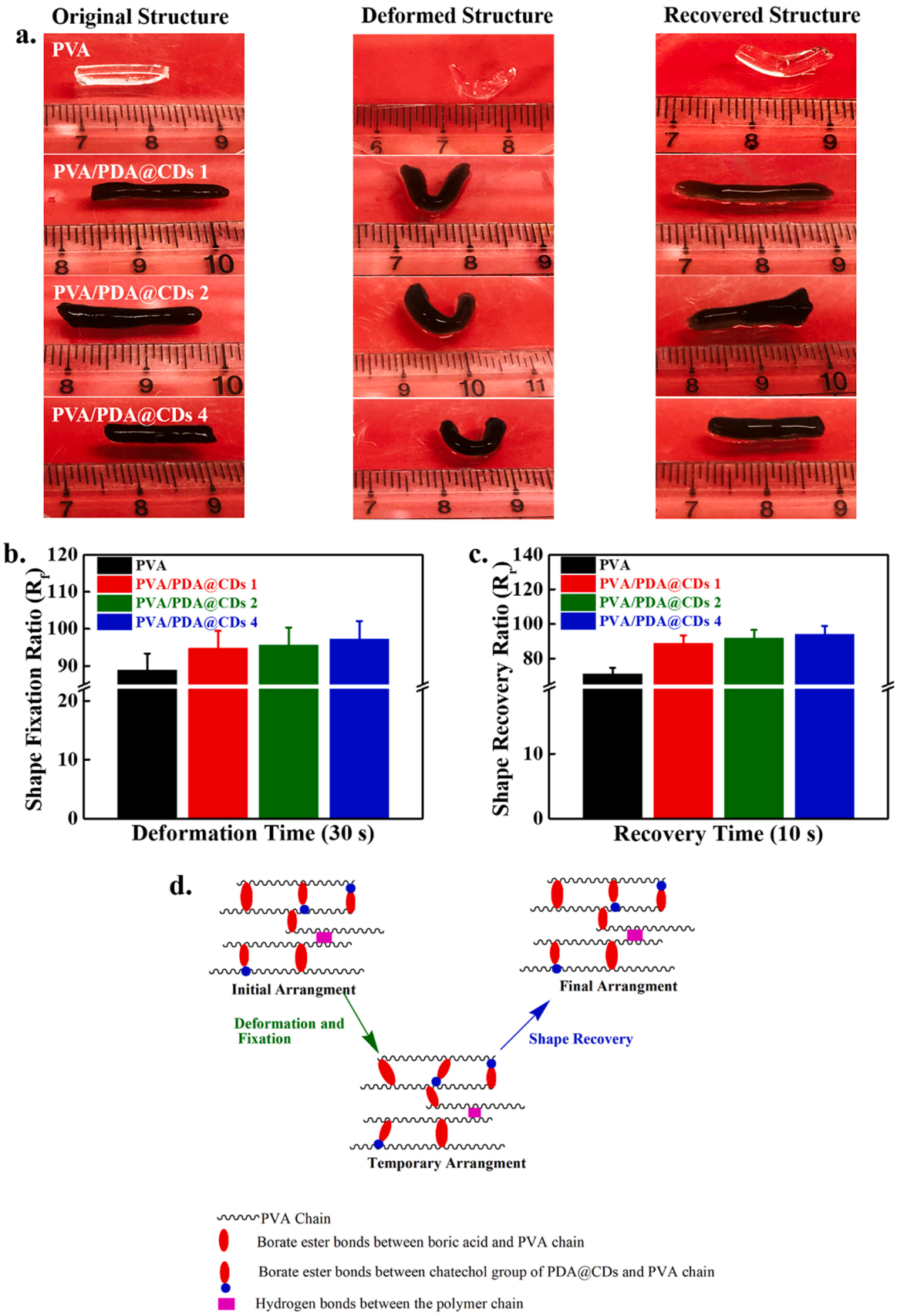

Fig. 7. Examination of shape recovery potential in the developed hydrogels. (a) Photographs of the hydrogel before and after shape recovery, (b) Quantitative value of shape fixation ability of the developed hydrogels, (c) Quantitative value of shape recovery potential of the developed hydrogels, and (d) Possible mechanism for shape deformation and shape recovery.

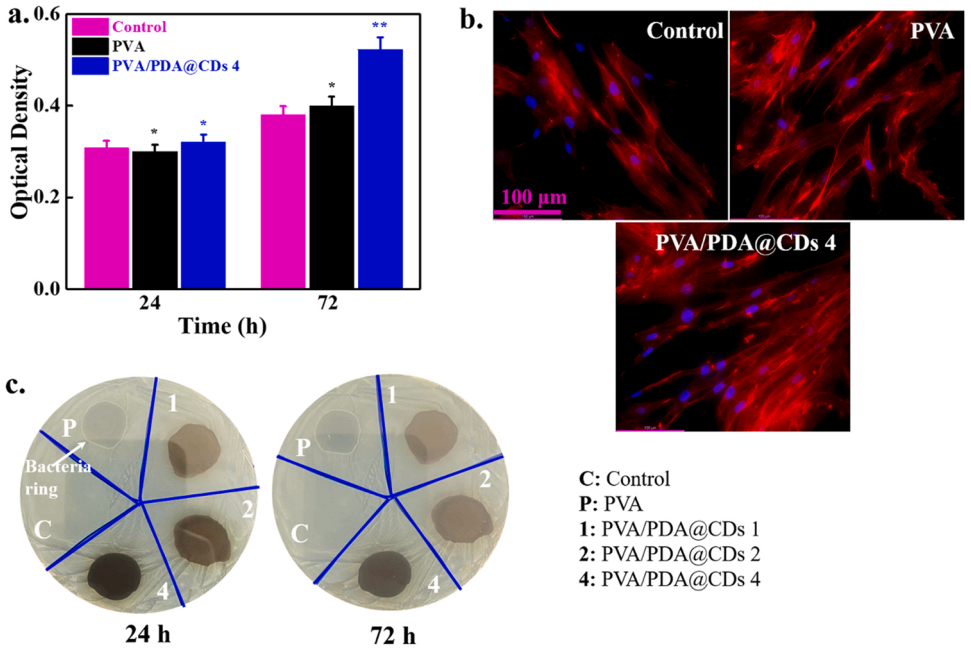

Fig. 8. Cytotoxicity and antibacterial evaluations of the developed hydrogels. (a) Viability of HDFs cells with developed hydrogels at indicated periods, (b) Fluorescence images of HDFs cells after 24 h of incubation with indicated hydrogels, and (c) Antibacterial activity of the developed hydrogels at indicated periods.

The groups without hydrogel treatment were served as control. Here, we chose PVA/PDA@CDs 4 hydrogel to examine its cytotoxicity with PVA hydrogel and control due to its superior physicochemical properties (mechanical strength, recovery, adhesive strength, and conductivity) over other hydrogels. No adverse effects were observed in the hydrogels treated groups, showing their biocompatibility. However, a slight increase in cell viability was observed after 24 h of incubation in PVA/PDA@CDs hydrogel treated groups than others, which significantly increased after 72 h of treatment, demonstrating its improved biocompatibility. The biocompatibility of the PVA hydrogel has been reported earlier [62]. The improved biocompatibility in PVA/PDA@CDs 4 hydrogel than PVA hydrogel and control can be attributed to the presence of PDA@CDs, which favored cellular activity by absorbing serum on the surface [29]. The morphologies of HDFs were also examined after 24 h incubation, and the obtained images are shown in (Fig. 8b). The cells were elongated and in healthy condition, showing the biocompatibility of the hydrogels. Cell densities were high in PVA/PDA@CDs 4 treated groups than others, suggesting their superior biocompatibility. Therefore, it could be a nontoxic material for sensing devices and biomedical applications.

The bacterial infection is a common process for wearable electronic devices, which causes inflammations and other diseases on the contact skin. Thus, the antibacterial potential in wearable electronic devices is highly desirable for preventing allergic symptoms. The antibacterial potential of the developed hydrogels was monitored with *Escherichia coli* after 24 and 72 h of incubation, and the obtained results are shown in (Fig. 8c). The experimental sites without hydrogel treatment were considered as control. No bacterial colonies were observed on the surface of hydrogels after 24 h of treatment, showing their antibacterial potential. The formation of bacterial colonies was observed around the pure polymer hydrogel.

In contrast, no such appearance occurred with composite hydrogels after 24 and 72 h of incubation, demonstrating zone inhibitory efficiency of the hydrogels. The improved antibacterial activity of the composite hydrogels can be attributed to the presence of catechol, and secondary amine functional groups in PDA@CDs, which denatured bacteria cell membrane protein leading to the death of bacteria. This finding indicates that the developed hydrogels can be utilized for wearable electronic devices without bacterial growth.

3.9. Electrochemical and sensing behavior of hydrogels

Conductivity is an essential parameter in sensing applications. We measured the resistance of the developed hydrogels using a four-point probe method, and the results are presented in (Fig. 9a). An improvement in the conductivity (0.57 → 1.46 mS/cm) was observed in the composite hydrogels than the pure polymer hydrogel. The enhancement in the conductivity of the composite hydrogels can be attributed to the presence of conductive CDs in the polymer matrix. The enhancement in the conductivity of CDs incorporated electrochemical devices have been reported earlier [63]. It is anticipated that the composite hydrogels have more interconnected network structures than pure polymer hydrogels, which facilitate the transport and diffusion of electrons, molecules, and ions leading to improve conductivity [64]. The formation of more interconnected network structures is supported by the recovery measurement, where greater recovery potential was observed in composite hydrogels than the pure polymer hydrogel due to the strong interactions. The PVA/PDA@CDs 4 hydrogel conductivity is also shown by illuminating the LED bulbs. Here, we chose PVA/PDA@CDs 4 hydrogel to show the illumination property due to its improved conductivity than other hydrogels. The image of the illuminated LED bulb is shown in (Fig. 9b). A bright illumination was observed with the developed hydrogel, showing its superior conductivity. Furthermore, the conductivity of the hydrogels was examined by toughening a mobile phone display. The images of the mobile display before and after hydrogel contact are shown in (Fig. 9c). The mobile display became active after contact with the hydrogel, revealing its conductive character. This result indicated that the developed hydrogels have the potential and can be utilized to fabricate electronic skin to dial a smartphone number. A video file to demonstrate the dialing capacity of the hydrogel is provided in **Video S1**.

Supplementary material related to this article can be found online at doi:10.1016/j.mtcomm.2022.103906.

The electrochemical performance of PVA/PDA@CDs hydrogel was examined through cyclic voltammetry with different scan rates (1, 2, 5, and 50 mV/sec) in the range of (−0.5) – (−0.1) V, and the obtained curves are given in (Fig. 9d). Here, we chose only PVA/PDA@CDs hydrogel to examine its CV behavior due to its superior conductivity to other hydrogels. Nearly a rectangular CV curve was observed at the

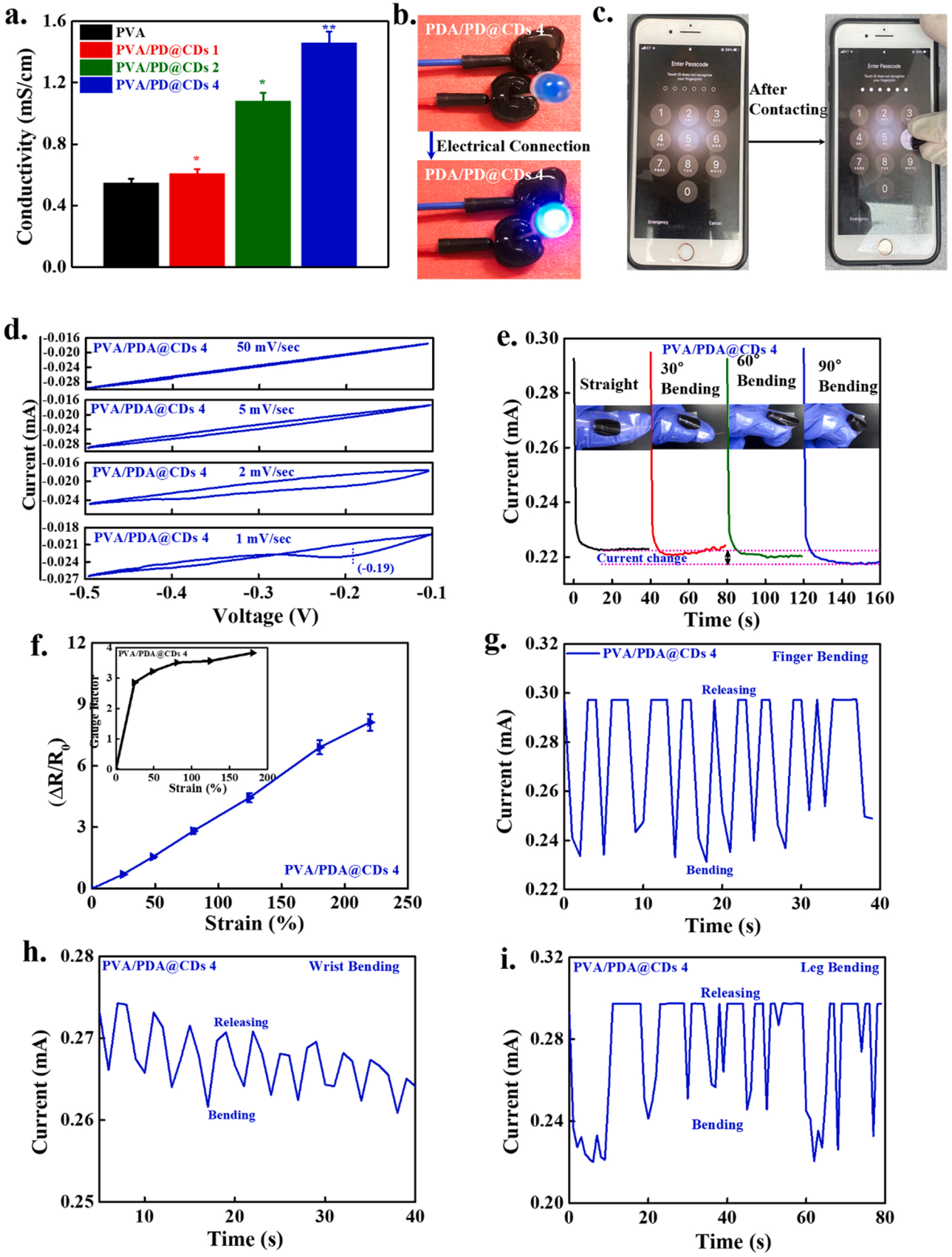

Fig. 9. Evaluation of the electrochemical and sensing potentials of the developed hydrogels. (a) Conductivity measurement of the developed hydrogels ($n = 3$) at $^{*}p < 0.05$, & $^{**}p < 0.01$, (b) Illumination of LED bulbs with indicated hydrogels, (c) Change in the mobile display after contact with the hydrogel, (d) CV curves of the indicated hydrogels at different scan rates (1, 2, 5, and 50 mV/s), (e) Change in the hydrogel current value at different angles, (f) change in the relative resistance of the hydrogel and GF value (inset), and (g-i) motion sensing potential of the indicated hydrogels with different parts of human body, *i.e.* finger, wrist, and knee.

lower scan rate with an increased area than the high scan rate (50 mV/sec), suggesting their specific capacitance potential. The decrease in the CV area at a high scan rate can be attributed to insufficient transfer of the reactive functional groups/ions at electrode surfaces due to the rapid change in the voltage. The increase in CV area at the lower scan rates can be assigned to the favorable active groups/ions movements within hydrogel solution, causing greater availability of groups at the electrode surfaces. Additionally, hydrogels also exhibited a redox peak at − 0.19 V at 1 mV/sec, attributed to the presence of electroactive PDA@CDs in the polymer matrix [65]. This peak disappeared with increasing scan rates due to the hindrance in transferring active functional groups/ions. Thus, selecting a suitable scan rate is required for optimum electrochemical performances.

The developed hydrogels exhibited superior adhesive, self-healing, and conductive properties, making them an ideal material for fabricating flexible wearable electronic devices for sensing applications [66, 67]. To use as flexible wearable devices, we monitored the adhesive behavior of the developed hydrogels on the human index finger, and the result is shown in **Video S2.** Adhesiveness is required for wearable sensing applications, and the developed hydrogel has firmly adhered to the index finger during the motion. Before measuring the sensing characteristics of the PVA/PDA@CDs 4 hydrogels, we examined the changes in the current of the hydrogel at different bending conditions, and the results are shown in (Fig. 9e). The dimensions of the hydrogel were 21.76 mm × 7.44 mm (length: width). We chose PVA/PDA@CDs 4 hydrogel for sensing application, due to its improved conductivity. We measured the current value at 0, 30, 60, and 90° bending of the finger.

Supplementary material related to this article can be found online at doi:10.1016/j.mtcomm.2022.103906.

No significant change in the current was observed under static conditions. However, a systematic decrease in the hydrogel current was observed by increasing the bending angle of finger. A decrease in the current is attributed to an increase in the hydrogel resistance during bending condition. The relative resistance change and sensitivity (gauge factor) of the hydrogel is given in (Fig. 9f). A systematic enhancement in the resistance was observed with increasing the strain in the hydrogel, showing minimization of the internal conductive pathway with stretching. Additionally, the GF was increased with increasing the strain, and it was 3.8 at 180% stretching, demonstrating good sensitivity. The obtained GF value was higher than the previously reported strain sensors using highly conductive graphene or polyaniline in the polymer matrix [68]. The developed hydrogel observed a real-time finger/-wrist/leg motion of the human body for practical application in healthcare examinations. The change in the hydrogel current under normal and bending conditions applied to the human finger is shown in (Fig. 9g). Nearly the uniform waveforms were observed during the finger motion, showing its potential for motion sensing. The magnitude of current change was profoundly affected by the bending activity of the finger. The bending condition has a lower current value due to the higher resistance of the hydrogel. A high bending causes a greater reduction in the current value.

Similarly, we also examined the motion-sensing behavior of the hydrogel with different parts of the human body (wrist and knee) to validate our findings, and the results are presented in (Fig. 9h-i). The hydrogel generates the waveforms during the motion of the applied body parts, and the magnitude of the generated waveforms depends on the bending of the body parts. A movie file for rapid motion sensing application with the developed hydrogel is given in **Video S3.** Rapid changes in current values occurred with the finger motion, and the generated waveforms exhibited nearly identical current values. A comparative study with previously reported works is also summarized in Table 2**.** These findings suggested that the developed hydrogels have the potential and can be explored for sensing applications.

Supplementary material related to this article can be found online at doi:10.1016/j.mtcomm.2022.103906.

Table 2
An overview of hydrogel-based strain sensors in previously reported works.

System	Advantage	Limitation	Ref.
Polyvinyl alcohol/o-carboxymethyl chitosan/poly (β-cyclodextrin)/ carbon nanotubes	Self-healing, adhesive, conductive, and biocompatible	NIR responsiveness not mentioned	[28]
Polyacrylic acid/ methacrylated chitosan/Tara tannin	Good mechanical strength, self-healing, adhesive, and conductive	Antibacterial and NIR responsiveness not mentioned	[14]
Polyvinyl alcohol/ sodium alginate/ tannic acid	Good mechanical strength, self-healing, conductive and biocompatible	Recovery, antibacterial, and NIR responsiveness not mentioned	[15]
Polyvinyl alcohol/ β-cyclodextrin/ carbon nanotubes	Self-healing, stretchable, conductive, and biocompatible	Recovery, antibacterial, and NIR responsiveness not mentioned	[25]
Sodium alginate/ acrylic acid/ aminated gelatin/ aluminum chloride	Good mechanical strength, self-healing, adhesive, conductive, and biocompatible	NIR responsiveness not mentioned	[26]
Polyvinyl alcohol/ polydopamine/ carbon dots	**Bio-waste material as conductive source**, improved mechanical strength, adhesive, self-healing, conductive, stretchable, **NIR responsiveness**, **antibacterial**, and biocompatible with good sensitivity (**Gauge factor = 3.8 at 180% strain**)	–	This work

4. Conclusion

Multifunctional hydrogels of PVA were synthesized using PDA modified CDs (PDA@CDs) for strain-sensing applications. The CDs were synthesized from cucumber peels through heat treatment. PDA functionalization with CDs was performed under alkaline conditions *via in situ* polymerization of dopamine. The composite hydrogels exhibited superior mechanical, rheological, and adhesive properties compared to those of the pure polymer hydrogel. The developed hydrogels exhibited self-healing and photothermal activity. A significant increase in temperature was observed by NIR irradiation within 20 s, showing the enhanced photothermal conversion efficiency of the hydrogels. The biocompatibility of the developed hydrogels was evaluated with HDFs cells. No adverse effects were detected on HDFs vitality with the developed hydrogels, suggesting their biocompatibility. The developed hydrogels demonstrated antibacterial potential, providing additional advantages in developing wearable electronic devices for different applications.

The developed hydrogels exhibited conductive property, which was profoundly affected by PDA@CDs contents. No significant variation in the hydrogel current was observed under static conditions. In comparison, a decrease in the current value occurred during bending due to increased hydrogel resistance. The motion-sensing ability of the hydrogel was monitored at different parts of the human body (finger, wrist, and knee), and nearly uniform patterns were generated through the hydrogel, showing their sensing ability. We anticipate that the developed hydrogels are multipotent and can be explored for strain-sensing applications. However, more detailed studies are required to validate our findings for practical applications of the developed hydrogels.

CRediT authorship contribution statement

Dinesh K. Patel: Conceptualization, Fabrication, Characterizations, Manuscript writing. **Keya Ganguly:** Characterizations, Analysis. **Sayan Deb Dutta:** Characterizations, Analysis. **Tejal V. Patil:** Characterizations, Analysis. **Ki-Taek Lim:** Supervision, Funding acquisition, Project administration, Writing – review & editing.

Declaration of Competing Interest

The authors declare that they have no known competing financial interests or personal relationships that could have appeared to influence the work reported in this paper.

Data Availability

The data used to support the findings of this study are available from the corresponding author upon request.

Acknowledgments

The Basic Science Research Program supported this work through the National Research Foundation of Korea (NRF) funded by the Ministry of Education (No. 2018R1A6A1A03025582, 2019R1D1A3A03103828 & 2022R1I1A3063302), Republic of Korea. The authors also acknowledge the Korean Basic Science Institute (KBSI), Chuncheon, Republic of Korea, providing FE-TEM facility.

Appendix A. Supplementary material

Supplementary data associated with this article can be found in the online version at doi:10.1016/j.mtcomm.2022.103906.

References

[1] M.A. Darabi, A. Khosrozadeh, R. Mbeleck, Y. Liu, Q. Chang, J. Jiang, J. Cai, Q. Wang, G. Luo, M. Xing, Skin-inspired multifunctional autonomic-intrinsic conductive self-healing hydrogels with pressure sensitivity, stretchability, and 3D printability, Adv. Mater. 29 (2017), 1700533.
[2] F. Lin, Z. Wang, Y. Shen, L. Tang, P. Zhang, Y. Wang, Y. Chen, B. Huang, B. Lu, Natural skin-inspired versatile cellulose biomimetic hydrogels, J. Mater. Chem. A 7 (2019) 26442–26455.
[3] T.R. Ray, J. Choi, A.J. Bandodkar, S. Krishnan, P. Gutruf, L. Tian, R. Ghaffari, J. A. Rogers, Bio-integrated wearable systems: a comprehensive review, Chem. Rev. 119 (2019) 5461–5533.
[4] I. Hwang, H.N. Kim, M. Seong, S.-H. Lee, M. Kang, H. Yi, W.G. Bae, M.K. Kwak, H. E. Jeong, Multifunctional smart skin adhesive patches for advanced health care, Adv. Healthc. Mater. 7 (2018), 1800275.
[5] W. Gao, S. Emaminejad, H.Y.Y. Nyein, S. Challa, K. Chen, A. Peck, H.M. Fahad, H. Ota, H. Shiraki, D. Kiriya, D.-H. Lien, G.A. Brooks, R.W. Davis, A. Javey, Fully integrated wearable sensor arrays for multiplexed in situ perspiration analysis, Nature 529 (2016) 509–514.
[6] J.-W. Jeong, W.-H. Yeo, A. Akhtar, J.J.S. Norton, Y.-J. Kwack, S. Li, S.-Y. Jung, Y. Su, W. Lee, J. Xia, H. Cheng, Y. Huang, W.-S. Choi, T. Bretl, J.A. Rogers, Materials and optimized designs for human-machine interfaces via epidermal electronics, Adv. Mater. 25 (2013) 6839–6846.
[7] Y. Wang, L. Zhang, A. Lu, Highly stretchable, transparent cellulose/PVA composite hydrogel for multiple sensing and triboelectric nanogenerators, J. Mater. Chem. A 8 (2020) 13935–13941.
[8] C. Keplinger, J.-Y. Sun, C.C. Foo, P. Rothemund, G.M. Whitesides, Z. Suo, Stretchable, transparent, ionic conductors, Science 341 (2013) 984–987.
[9] Y. Li, Y.A. Samad, K. Liao, From cotton to wearable pressure sensor, J. Mater. Chem. A 3 (2015) 2181–2187.
[10] S.R. Shin, B. Aghaei-Ghareh-Bolagh, T.T. Dang, S.N. Topkaya, X. Gao, S.Y. Yang, S. M. Jung, J.H. Oh, M.R. Dokmeci, X.S. Tang, A. Khademhosseini, Cell-laden microengineered and mechanically tunable hybrid hydrogels of gelatin and graphene oxide, Adv. Mater. 25 (2013) 6385–6391.
[11] N. Varshney, A.K. Sahi, S. Poddar, N.K. Vishwakarma, G. Kavimandan, A. Prakash, S.K. Mahto, Freeze–thaw-induced physically cross-linked superabsorbent polyvinyl alcohol/soy protein isolate hydrogels for skin wound dressing: in vitro and in vivo characterization, ACS Appl. Mater. Interfaces 14 (2022) 14033–14048.
[12] N.D. Thorat, K.P. Shinde, S.H. Pawar, K.C. Barick, C.A. Betty, R.S. Ningthoujam, Polyvinyl alcohol: an efficient fuel for synthesis of superparamagnetic LSMO nanoparticles for biomedical application, Dalton Trans. 41 (2012) 3060.
[13] Z. Miao, Y. Sun, Z. Tao, Y. Chen, Y. Ma, D. Zhu, X. Huang, Z. Zha, Thermochromic polyvinyl alcohol-iodine hydrogels with safe threshold temperature for infectious wound healing, Adv. Healthc. Mater. 10 (2021), 2100722.
[14] J. Liu, S. Bao, Q. Ling, X. Fan, H. Gu, Ultra-fast preparation of multifunctional conductive hydrogels with high mechanical strength, self-healing and self-adhesive properties based on Tara Tannin-Fe^{3+} dynamic redox system for strain sensors applications, Polymer 240 (2022), 124513.
[15] L. Zhao, Z. Ren, X. Liu, Q. Ling, Z. Li, H. Gu, A multifunctional, self-healing, self-adhesive, and conductive sodium alginate/poly(vinyl alcohol) composite hydrogel as a flexible strain sensor, ACS Appl. Mater. Interfaces 13 (2021) 11344–11355.
[16] Y. Yu, X. Zhao, L. Ye, A new mussel-inspired highly self-adhesive & conductive poly (vinyl alcohol)-based hydrogel for wearable sensors, Appl. Surf. Sci. 562 (2021), 150162.
[17] H. Lee, N.F. Scherer, P.B. Messersmith, Single-molecule mechanics of mussel adhesion, Proc. Natl. Acad. Sci. 103 (2006) 12999–13003.
[18] X. Zeng, M. Luo, G. Liu, X. Wang, W. Tao, Y. Lin, X. Ji, L. Nie, L. Mei, Polydopamine-modified black phosphorous nanocapsule with enhanced stability and photothermal performance for tumor multimodal treatments, Adv. Sci. 5 (2018), 1800510.
[19] X. Cao, H. Liu, X. Yang, J. Tian, B. Luo, M. Liu, Halloysite nanotubes@ polydopamine reinforced polyacrylamide-gelatin hydrogels with NIR light triggered shape memory and self-healing capability, Compos. Sci. Technol. 191 (2020), 108071.
[20] F. Liu, X. Liu, H. Gu, Multi-network poly(β-cyclodextrin)/PVA/Gelatin/carbon nanotubes composite hydrogels constructed by multiple dynamic crosslinking as flexible electronic devices, Macromol. Mater. Eng. 307 (2021), 2100724.
[21] A. Konwar, U. Baruah, M.J. Deka, A.A. Hussain, S.R. Haque, A.R. Pal, D. Chowdhury, Tea-carbon dots-reduced graphene oxide: an efficient conducting coating material for fabrication of an E-textile, ACS Sustain. Chem. Eng. 5 (2017) 11645–11651.
[22] H. Qi, M. Teng, M. Liu, S. Liu, J. Li, H. Yu, C. Teng, Z. Huang, H. Liu, Q. Shao, A. Umar, T. Ding, Q. Gao, Z. Guo, Biomass-derived nitrogen-doped carbon quantum dots: highly selective fluorescent probe for detecting Fe^{3+} ions and tetracyclines, J. Colloid Interface Sci. 539 (2019) 332–341.
[23] R. Das, R. Bandyopadhyay, P. Pramanik, Carbon quantum dots from natural resource: a review, Mater. Today Chem. 8 (2018) 96–109.
[24] Y. Wang, J. Sun, B. He, M. Feng, Synthesis and modification of biomass derived carbon dots in ionic liquids and their application: a mini review, Green Chem. Eng. 1 (2020) 94–108.
[25] X. Liu, Z. Ren, F. Liu, L. Zhao, Q. Ling, H. Gu, Multifunctional self-healing dual network hydrogels constructed via host–guest interaction and dynamic covalent bond as wearable strain sensors for monitoring human and organ motions, ACS Appl. Mater. Interfaces 13 (2021) 14612–14622.
[26] L. Zhao, T. Ke, Q. Ling, J. Liu, Z. Li, H. Gu, Multifunctional ionic conductive double-network hydrogel as a long-term flexible strain sensor, ACS Appl. Polym. Mater. 3 (2021) 5494–5508.
[27] Q. Ling, T. Ke, W. Liu, Z. Ren, L. Zhao, H. Gu, Tough, repeatedly adhesive, cyclic compression-stable, and conductive dual-network hydrogel sensors for human health monitoring, Ind. Eng. Chem. Res. 60 (2021) 18373–18383.
[28] Z. Ren, T. Ke, Q. Ling, L. Zhao, H. Gu, Rapid self-healing and self-adhesive chitosan-based hydrogels by host-guest interaction and dynamic covalent bond as flexible sensor, Carbohydr. Polym. 273 (2021), 118533.
[29] X. Jing, H.-Y. Mi, Y.-J. Lin, E. Enriquez, X.-F. Peng, L.-S. Turng, Highly stretchable and biocompatible strain sensors based on mussel-inspired super-adhesive self-healing hydrogels for human motion monitoring, ACS Appl. Mater. Interfaces 10 (2018) 20897–20909.
[30] H. Rammal, A. GhavamiNejad, A. Erdem, R. Mbeleck, M. Nematollahi, S. Emir Diltemiz, H. Alem, M.A. Darabi, Y.N. Ertas, E.J. Caterson, N. Ashammakhi, Advances in biomedical applications of self-healing hydrogels, Mater. Chem. Front. 5 (2021) 4368–4400.
[31] S.K. Bhunia, A. Saha, A.R. Maity, S.C. Ray, N.R. Jana, Carbon nanoparticle-based fluorescent bioimaging probes, Sci. Rep. 3 (2013) 01473.
[32] Z. Li, H. Xu, J. Shao, C. Jiang, F. Zhang, J. Lin, H. Zhang, J. Li, P. Huang, Polydopamine-functionalized black phosphorus quantum dots for cancer theranostics, Appl. Mater. Today 15 (2019) 297–304.
[33] H. Jing, L. He, J. Feng, H. Fu, S. Guan, P. Guo, High strength hydrogels with multiple shape-memory ability based on hydrophobic and electrostatic interactions, Soft Matter 15 (2019) 5264–5270.
[34] S. Cometta, N. Bock, S. Suresh, T.R. Dargaville, D.W. Hutmacher, Antibacterial albumin-tannic acid coatings for scaffold-guided breast reconstruction, Front. Bioeng. Biotechnol. 9 (2021), 638577.
[35] J. Zhou, Z. Sheng, H. Han, M. Zou, C. Li, Facile synthesis of fluorescent carbon dots using watermelon peel as a carbon source, Mater. Lett. 66 (2012) 222–224.
[36] S. Eigler, C. Dotzer, A. Hirsch, Visualization of defect densities in reduced graphene oxide, Carbon 50 (2012) 3666–3673.
[37] D.C. Marcano, D.V. Kosynkin, J.M. Berlin, A. Sinitskii, Z. Sun, A. Slesarev, L. B. Alemany, W. Lu, J.M. Tour, Improved synthesis of graphene oxide, ACS Nano 4 (2010) 4806–4814.
[38] H. Kim, Y. Miura, C.W. Macosko, Graphene/polyurethane nanocomposites for improved gas barrier and electrical conductivity, Chem. Mater. 22 (2010) 3441–3450.
[39] Z. Li, J. Ni, L. Liu, L. Gu, Z. Wu, T. Li, K.I. Ivanovich, W. Zhao, T. Sun, T. Wang, Imaging-guided chemo–photothermal polydopamine carbon dots for EpCAM-targeted delivery toward liver tumor, ACS Appl. Mater. Interfaces 13 (2021) 29340–29348.

[40] Q. Chang, Z. Guo, Z. Shen, N. Li, C. Xue, H. Zhang, C. Hao, J. Yang, S. Hu, Interaction promotes the formation and photothermal conversion of carbon dots/polydopamine composite for solar-driven water evaporation, Adv. Mater. Interfaces 8 (2021), 2100332.
[41] S. Wei, W. Lu, X. Le, C. Ma, H. Lin, B. Wu, J. Zhang, P. Theato, T. Chen, Bioinspired synergistic fluorescence-color-switchable polymeric hydrogel actuators, Angew. Chem. Int. Ed. 58 (2019) 16243–16251.
[42] T. Jayaramudu, H.-U. Ko, H. Kim, J. Kim, R. Muthoka, J. Kim, Electroactive hydrogels made with polyvinyl alcohol/cellulose nanocrystals, Materials 11 (2018) 1615.
[43] Y. Liu, L.M. Geever, J.E. Kennedy, C.L. Higginbotham, P.A. Cahill, G. B. McGuinness, Thermal behavior and mechanical properties of physically crosslinked PVA/gelatin hydrogels, J. Mech. Behav. Biomed. Mater. 3 (2010) 203–209.
[44] S.-H. Hwang, D. Kang, R.S. Ruoff, H.S. Shin, Y.-B. Park, Poly(vinyl alcohol) reinforced and toughened with poly(dopamine)-treated graphene oxide, and its use for humidity sensing, ACS Nano 8 (2014) 6739–6747.
[45] Y.-F. Tang, Y.-M. Du, X.-W. Hu, X.-W. Shi, J.F. Kennedy, Rheological characterisation of a novel thermosensitive chitosan/poly(vinyl alcohol) blend hydrogel, Carbohydr. Polym. 67 (2007) 491–499.
[46] J. Han, T. Lei, Q. Wu, High-water-content mouldable polyvinyl alcohol-borax hydrogels reinforced by well-dispersed cellulose nanoparticles: dynamic rheological properties and hydrogel formation mechanism, Carbohydr. Polym. 102 (2014) 306–316.
[47] L. Zhu, J. Qiu, E. Sakai, A high modulus hydrogel obtained from hydrogen bond reconstruction and its application in vibration damper, RSC Adv. 7 (2017) 43755–43763.
[48] X. He, C. Zhang, M. Wang, Y. Zhang, L. Liu, W. Yang, An electrically and mechanically autonomic self-healing hybrid hydrogel with tough and thermoplastic properties, ACS Appl. Mater. Interfaces 9 (2017) 11134–11143.
[49] M.D. Hager, P. Greil, C. Leyens, S. van der Zwaag, U.S. Schubert, Self-healing materials, Adv. Mater. 22 (2010) 5424–5430.
[50] Y. Tu, N. Chen, C. Li, H. Liu, R. Zhu, S. Chen, Q. Xiao, J. Liu, S. Ramakrishna, L. He, Advances in injectable self-healing biomedical hydrogels, Acta Biomater. 90 (2019) 1–20.
[51] R.E. Abouzeid, R. Khiari, D. Beneventi, A. Dufresne, Biomimetic mineralization of three-dimensional printed alginate/TEMPO-oxidized cellulose nanofibril scaffolds for bone tissue engineering, Biomacromolecules 19 (2018) 4442–4452.
[52] J.C. Yeo, H.K. Yap, W. Xi, Z. Wang, C.-H. Yeow, C.T. Lim, Flexible and stretchable strain sensing actuator for wearable soft robotic applications, Adv. Mater. Technol. 1 (2016), 1600018.
[53] M.K. Kwak, H.-E. Jeong, K.Y. Suh, Rational design and enhanced biocompatibility of a dry adhesive medical skin patch, Adv. Mater. 23 (2011) 3949–3953.
[54] S. Liu, R. Zheng, S. Chen, Y. Wu, H. Liu, P. Wang, Z. Deng, L. Liu, A compliant, self-adhesive and self-healing wearable hydrogel as epidermal strain sensor, J. Mater. Chem. C 6 (2018) 4183–4190.
[55] L. Han, X. Lu, M. Wang, D. Gan, W. Deng, K. Wang, L. Fang, K. Liu, C.W. Chan, Y. Tang, L.-T. Weng, H. Yuan, A mussel-inspired conductive, self-adhesive, and self-healable tough hydrogel as cell stimulators and implantable bioelectronics, Small 13 (2017), 1601916.
[56] J. Qu, X. Zhao, Y. Liang, T. Zhang, P.X. Ma, B. Guo, Antibacterial adhesive injectable hydrogels with rapid self-healing, extensibility and compressibility as wound dressing for joints skin wound healing, Biomaterials 183 (2018) 185–199.
[57] X. Pei, H. Zhang, Y. Zhou, L. Zhou, J. Fu, Stretchable, self-healing and tissue-adhesive zwitterionic hydrogels as strain sensors for wireless monitoring of organ motions, Mater. Horiz. 7 (2020) 1872–1882.
[58] Z. Sun, C. Song, J. Zhou, C. Hao, W. Liu, H. Liu, J. Wang, M. Huang, S. He, M. Yang, Rapid photothermal responsive conductive MXene nanocomposite hydrogels for soft manipulators and sensitive strain sensors, Macromol. Rapid Commun. 42 (2021), 2100499.
[59] B. Zhou, Z. Guo, Z. Lin, L. Zhang, B.-P. Jiang, X.-C. Shen, Recent insights into near-infrared light-responsive carbon dots for bioimaging and cancer phototherapy, Inorg. Chem. Front. 6 (2019) 1116–1128.
[60] G. Xiao, Y. Wang, H. Zhang, Z. Zhu, S. Fu, Cellulose nanocrystal mediated fast self-healing and shape memory conductive hydrogel for wearable strain sensors, Int. J. Biol. Macromol. 170 (2021) 272–283.
[61] X. Xiong, J. Sun, D. Hu, C. Xiao, J. Wang, Q. Zhuo, C. Qin, L. Dai, Fabrication of polyvinyl alcohol hydrogels with excellent shape memory and ultraviolet-shielding behavior via the introduction of tea polyphenols, RSC Adv. 10 (2020) 35226–35234.
[62] L. Jing, H. Li, R.Y. Tay, B. Sun, S.H. Tsang, O. Cometto, J. Lin, E.H.T. Teo, A.I. Y. Tok, Biocompatible hydroxylated boron nitride nanosheets/poly(vinyl alcohol) interpenetrating hydrogels with enhanced mechanical and thermal responses, ACS Nano 11 (2017) 3742–3751.
[63] H.J. Won, B. Ryplida, S.G. Kim, G. Lee, J.H. Ryu, S.Y. Park, Diselenide-bridged carbon-dot-mediated self-healing, conductive, and adhesive wireless hydrogel sensors for label-free breast cancer detection, ACS Nano 14 (2020) 8409–8420.
[64] Z. Wang, F. Cheng, H. Cai, X. Li, J. Sun, Y. Wu, N. Wang, Y. Zhu, Robust versatile nanocellulose/polyvinyl alcohol/carbon dot hydrogels for biomechanical sensing, Carbohydr. Polym. 259 (2021), 117753.
[65] L.C. Almeida, T. Frade, R.D. Correia, Y. Niu, G. Jin, J.P. Correia, A.S. Viana, Electrosynthesis of polydopamine-ethanolamine films for the development of immunosensing interfaces, Sci. Rep. 11 (2021) 2237.
[66] X. Zhou, A. Rajeev, A. Subramanian, Y. Li, N. Rossetti, G. Natale, G.A. Lodygensky, F. Cicoira, Self-healing, stretchable, and highly adhesive hydrogels for epidermal patch electrodes, Acta Biomater. 139 (2021) 296–306.
[67] C. Zheng, K. Lu, Y. Lu, S. Zhu, Y. Yue, X. Xu, C. Mei, H. Xiao, Q. Wu, J. Han, A stretchable, self-healing conductive hydrogels based on nanocellulose supported graphene towards wearable monitoring of human motion, Carbohydr. Polym. 250 (2020), 116905.
[68] Z. Wang, H. Zhou, J. Lai, B. Yan, H. Liu, X. Jin, A. Ma, G. Zhang, W. Zhao, W. Chen, Extremely stretchable and electrically conductive hydrogels with dually synergistic networks for wearable strain sensors, J. Mater. Chem. C 6 (2018) 9200–9207.